This is a compilation of the responses already published in the public discussion. The line numbers could be slightly off due to changes in editing. A marked up manuscript where all the changes are visible is attached at the end of this compilation.

Reviewer 1:

1. The abstract mentions “static rf-field inhomogeneity”. This might be a simple typo. I do not know what a “static rf field” is.
We have decided to delete the term "static" in the abstract since we agree with the reviewer that all rf-fields are time dependent (with the rf-irradiation frequency) in the laboratory frame. In the rotating frame, however, rectangular pulses typically have a constant rf amplitude and the rf-field inhomogeneity is also time independent. Under MAS conditions, the sample rotates through different parts of the coil volume and different rf-field amplitudes if the field is not homogeneous leading to a time-dependence of the rf-field amplitude (with the MAS frequency) induced by rf-field inhomogeneities. In this manuscript, this time dependence of the rf-field amplitude due to MAS and rf-field inhomogeneities is not included. In addition, we replaced the term "static rf-field inhomogeneity" on line 342 by " the time-independent part of the rf-field inhomogeneity under MAS" and added a sentence (also in response to point 3) "We have not included phase- or amplitude-modulations generated by MAS due to rf-field inhomogeneity in our investigation." There we give references to papers by Levitt, Tekely and Reif where effects caused by such time-dependent modulations of phase or amplitude due to rf-field inhomogeneities are discussed.

2. Figure 1 compares analytical and numerical simulations of several three-spin tensor operators that may contribute to residual linewidths. However it is not very obvious, neither in the figure annotations, nor the captions, what the definitions of these operators are. This also applies to the text. For example at the top of page 7, an operator T_{00}(ntau_4) is specified but it is unclear to me what ntau_4 is. Maybe I missed something but I don’t find the definition or relevance of ntau_4. Similar problems occur in many places. The authors should give clear definitions (if necessary, in the SI, or literature references) for all the terms mentioned in the paper.
We follow in the definition of the three-spin spherical-tensor operators the ones proposed in A. Garon, R. Zeier, S.J. Glaser, Visualizing operators of coupled spin systems, Phys. Rev. A. 91 (2015) which was referenced on line 130 of the original manuscript. We have now added the reference to the caption of Fig. 1 and also after the expressions for the three-spin operators in the main text (line 155) where we added: "... tensor operators where we follow the definition and notation introduced in Ref. (Garon et al., 2015)." We hope that these modifications make this part more understandable and the definition of the spherical-tensor operators clearer.

3. One point I would like clarifying is whether the only type of rf field imperfection that was considered was (possibly transient) errors in the rf amplitude. I am aware of two other imperfections that deserve consideration. First, phase errors are generated by a limited bandwidth probe when the input frequency is changed (as happens in a FSLG experiment). Early implementations of this method did use a relative phase adjustment of the two pulses to correct this effect (see http://www.sciencedirect.com/science/article/pii/B9780120255146500113). I wonder whether the more modern compensation algorithms already include such a phase correction (it is possible that this is so, but clarification is needed). The second feasible error is that spatial inhomogeneity in the direction of the radiofrequency field causes a periodic phase modulation as the sample rotates. NMR effects due to this have been detected in rotary resonance experiments (http://onlinelibrary.wiley.com/doi/10.1002/ijch.198800039/abstract). It is possible that such effects might also contribute to the residual linewidths.

We have corrected transient amplitude and transient phase errors in the transient-compensated implementation of the FSLG experiment. We checked the phase and amplitude of the rf pulses and found no significant deviations from the intended shape in the experimental implementation. The spatial homogeneity that translates to a time dependence under MAS was not considered in this

investigation. We have clarified this in the text on line 342 (see also above the response to point 1). We do not know whether such effects contribute to the residual line width but we plan to investigate them in the future.

Reviewer 2:

*It will be interesting to see how compensated cycles perform (even though the contribution the line width is marginal) for super-cycled FSLG/PMLG schemes where the effective axis is more along the z-axis. Does the supercycling minimise the third-order effect in any way or RF inhomogeneity?
The reason why we analyzed the performance of the basic FSLG sequence was the fact that the theoretical description is simpler than the one for the super-cycled versions and we wanted to be able to compare theory, experiments and simulations in order to gain as much insight as possible. Therefore, we did not yet look at super-cycled implementations and cannot give a definite answer to this question. We would prefer not to speculate about the effects of super cycling on these broadening mechanisms.

*The compensated schemes push the spectrum to lower ppm values. Is it totally right that transient compensated schemes yield spectra with absolute values of the frequency? For instance, in Figure 6, the shift is uniform, and unless one has the reference, it is impossible to say which gives the absolute values right. And if the reference is fixed, for a given spectrometer, under given conditions, the shift is always the same, unless the higher-order terms come into play for this as well. That is not very clear in the text.
The transient compensation leads to two effects that make the experiment more reproducible and the chemical shifts less arbitrary. The first is the better balancing of the forward and backward nutation in the FSLG experiment due to a better match of the rf-field amplitudes under phase ramps with positive and negative slopes. This part was actually missing and has been added to the manuscript (line 317) as "... to be due to the better compensation of the effective nutation over a full FSLG cycle and the additional ...". The second reason is the better elimination of fictitious fields as stated on line 318. This will not lead to absolute chemical shifts because the transient compensation is not perfect and especially the forward and backward nutation in the FSLG experiment will always produce some small residual effective nutation but this contribution is minimized by the transient compensation. We have changed the conclusions on line 435 to a more cautious formulation: "Removal of phase transients and adaption of the pulse sequence led to more predictable results in terms of chemical-shift scaling and smaller variations of the shift on the frequency axis.". We hope that this change makes it clearer that absolute frequency calibration is not possible even with transient compensation.

*The spectrum obtained with the compensated scheme, Figure 6, has certain artifacts like a shoulder for the NH3+, any comments.
We are not sure what the source of the shoulder is. The NH3 line of the compensated spectrum is slightly narrower and it could originate from some structure that starts to become visible. It could also be due to an artefact that shifts to a different spectral position in the compensated spectra. Since we do not know, we would prefer not to speculate about it.

*Any comments on the performance of these schemes at higher MAS, higher than 60 kHz. Also in the introduction when slow to medium MAS frequencies are mentioned, perhaps it is good to indicate what the frequencies are.
We have added a number to the text on line 33 to quantify the slow to medium MAS frequencies by adding "(slower than 60 kHz)". The exact number is debatable but we think that starting at 60 kHz averaging by MAS leads to some resolution in proton spectra. We have not looked at fast MAS experimentally and cannot comment on the performance under such conditions.

*Certain inconsistencies, I believe, like definition of tau_i (i=1 to 4) on pages 6 and 7, for instance.

We have added more references to "A. Garon, R. Zeier, S.J. Glaser, Visualizing operators of coupled spin systems, Phys. Rev. A. 91 (2015)" where the three-spin spherical tensor operators are defined. The caption of Fig. 1 was amended with the sentence: "For a definition of the three-spin spherical-tensor operators, see Ref. (Garon et al., 2015)." and after the expressions for the operators in the main text on line 155 we added: "... tensor operators where we follow the definition and notation introduced in Ref. (Garon et al., 2015).". We hope that this clarifies this point.

Reviewer 1 - 2nd response

With respect to point 3, most of the points are now clear. I do still wonder, however, precisely what is meant by "We checked the phase and amplitude of the rf pulses and found no significant deviations from the intended shape in the experimental implementation.". The issue here is exactly how the phase (in particular) was checked. The only reliable way to do this (that I am aware of) would be to use an antenna to pick up the rf generated in the coil itself. The phase of this would have to be determined by comparison with a reference wave with the same frequency (and which would also switch in frequency with the FSLG). Was this, or a similar procedure, used? I think the authors should clarify exactly how the phase and amplitude were checked, for a frequency-switched rf waveform driving a narrowband tuned circuit such as found in an NMR probe. If such a procedure were not used then the article should make it clearer that doubts remain about the frequency-dependent phase of the frequency-switched waveform, at the site of the NMR sample.

This is precisely how we checked the phases and amplitudes of the pulses. All probes where we can do transient compensation are equipped with a small pickup coil close to the NMR coil that can be used to measure the radio-frequency field. The coupling to the NMR coil is weak (about 40-50 dB) and we measure the voltage of the pickup coil with a fast digital scope (5-10 GS/s). The signal is then down sampled and mixed down in a phase-sensitive way using MATLAB so that we can determine the phase and the amplitude of the pulses with a high time resoultion. In this way, we can confirm that the transient-compensated pulses have indeed the intended amplitude shape with minor deviations. This procedure is described in (Wittmann et al., 2016) (J.J. Wittmann, V. Mertens, K. Takeda, B.H. Meier, M. Ernst, Quantification and compensation of the influence of pulse transients on symmetry-based recoupling sequences, J. Magn. Reson. 263 (2016) 7–18) where also examples of measured pulse shapes with transient compensation are shown. We hope that this answer makes the methods used to determine the experimental pulse shape at the site of the sample clearer.

Reviewer 3:

One aspect that didn't come across clearly was which spin parameters were significant in the third order terms, particularly in section 4 where heteronuclear couplings are now involved. Various spin operators are quoted, but it is not always clear whether these cross terms are arising from homonuclear dipolar couplings or heteronuclear dipolar couplings, cross-terms with offsets (or even 1H CSA). The analytical section refers to multiple three-spin operators, but presumably not all the contributions to the 3rd order terms will involve 3 spins?

We have added a sentence at line 155 where the second-order three-spin terms are discussed first to explain that these are commutator terms between two different dipolar couplings: " They all arise from commutators of one homonuclear dipolar coupling in the interaction frame of the effective field with another dipolar coupling where one spin is in common."

The third-order terms are of course more complex and we only discuss the ones that appear in situations where no second-order terms are found, i.e. in the two-spin system (line 170). Since there is only a single homonuclear dipolar coupling, they are double-commutator terms of this interaction with itself. We have modified a sentence on line 200 to make this clearer: "It is obvious from Figure 2 that the third-order terms (double commutator terms of a single homonuclear dipolar coupling in the interaction frame of the effective field) do not vanish under FSLG-irradiation ..."

We do not discuss at all cross terms with the CSA tensor since we believe that the dipolar couplings are the dominant interaction that determines the residual line width under homonuclear decoupling.

Hence, I found the discussion on P10 and P11 a bit confusing. What exactly is meant by "simulations with one and two dipolar couplings", a CH vs. a CH2 spin system or is it H3? Similarly, I had to read the caption of Fig 4 a couple of times, e.g. (A) and (B) are showing calculated splittings, rather than "simulations" or "Full scale linewidths". It would be better to say "without taking chemical-shift *scaling* into account" ("correction" is a bit vague and could refer to referencing).
When rereading this section, I have to agree that this was not very clearly formulated. We have modified the start of the discussion to make it clear that we talk about simulations in homonuclear three-spin systems where one or two dipolar couplings are non zero (line 242): " In order to validate the theoretical consideration of the pulse sequence, numerical simulations in a homonuclear three-spin systems were performed with both pulse implementations shown in Figure 3. To validate the contributions of second- and third-order terms discussed in the theory section, simulations using only one ($\delta_{12} \neq 0$) and two non-zero dipolar couplings ($\delta_{12} \neq 0,\ \delta_{13} \neq 0$) in a three-spin system were performed." We also amended the figure caption as suggested and added the homonuclear three-spin system to it to make it clearer.

Is Fig. 7 is showing 13C or 1H T2'? The sudden shift to heteronuclear systems is a little jarring. In this context, I must disagree with the characterisation in the introduction of our work on 3rd order contribution in heteronuclear systems (Tatton, 2012) as merely "qualitative"! There was greater emphasis on numerical simulation; analysis was confined to the simple LG, with the merit that simple expressions could be obtained for the 3rd order contributions, but it was certainly quantitative, and considered some of the same problems (influence of 13C heteronuclear couplings on 1H homonuclear decoupled spetra). So the two papers are nicely complementary; indeed the contribution of ~60 Hz to the linewidth agrees well with the earlier work, not just Fig S2!
The measurements are proton T2' and we have added this to the caption and the main text. We agree that qualitative is not a good characterization of ref. (Tatton, 2012) and have deleted the qualifier. We have also added, as suggested by the referee, that the observed heteronuclear broadening agrees well not only with Fig. S2 but also with literature results and added the reference on line 325.

Figure 8: Is a pi pulse being used in experimental spectra to refocus shift evolution in the indirect dimension? Were the simulations of the full 2D experiment or a 1D version? It will not affect the conclusions, but you wouldn't experiment the two versions of the experiment to match up quantitatively.
The experimental spectra are traces along the indirect dimension of a two-dimensional spectrum. No pi pulse was used in these measurements since we wanted to see spectra with chemical shifts which would be refocused by a pi pulse. The simulations are 1D simulations. The main reason for measuring 2D spectra was that we wanted to avoid windowed FSLG detection that produces additional artifacts. In simulations this is not a concern since detection can be implemented instantaneously.

Minor detail: Methanol and Ethanol in Materials and Methods should be lower case.
Corrected.

Origin of the Residual Linewidth Under FSLG-Based Homonuclear Decoupling in MAS Solid-State NMR

Johannes Hellwagner[1], Liam Grunwald[1], Manuel Ochsner[1], Daniel Zindel[1], Beat H. Meier[1], Matthias Ernst[1]

[1]Physical Chemistry, ETH Zürich, Zürich, 8093, Switzerland

Correspondence to: Matthias Ernst (maer@ethz.ch), Beat H. Meier (beme@ethz.ch)

Abstract. Homonuclear decoupling sequences in solid-state NMR under magic-angle spinning (MAS) show experimentally significantly larger residual linewidth than expected from Floquet theory to second order. We present an in-depth theoretical and experimental analysis of the origin of the residual linewidth in frequency-switched Lee-Goldburg (FSLG) based decoupling sequences. We analyze the effect of experimental pulse-shape errors (*e.g.* pulse transients and B_1-field inhomogeneities) and use a Floquet-theory based description of higher-order error terms that arise from the interference between the MAS rotation and the pulse sequence. It is shown that the magnitude of the third-order auto term of a single homo- or heteronuclear coupled spin pair is important and leads to significant line broadening under FSLG decoupling. Furthermore, we show the dependence of these third-order error terms on the angle of the effective field with the B_0 field. An analysis of second-order cross terms is presented that shows that the influence of three-spin terms is small since they are averaged by the pulse sequence. The importance of the rf-field inhomogeneity is discussed and shown to be the main source of residual line broadening while pulse transients do not seem to play an important role. Experimentally, the influence of the combination of these error terms is shown by using restricted samples and pulse-transient compensation. The results show that all terms are additive but the major contribution to the residual linewidth comes from the rf-field inhomogeneity for the standard implementation of FSLG sequences, which is significant even for samples with a restricted volume.

Deleted: static

1 Introduction

Protons are present in most materials and are one of the important nuclei in nuclear magnetic resonance (NMR) spectroscopy in the study of biological systems and materials. Besides the advantage of high sensitivity, protons allow insights into molecular packing in solids as direct observations of hydrogen bonding and C-H-π as well as π-π interactions are possible (Barfield, 2002; Berglund and Vaughan, 1980; Parker et al., 2006). While proton detection is routine in solution-state NMR, it is not yet used routinely in solid-state NMR due to the large proton-proton dipolar couplings that are only partially averaged out by magic-angle spinning (MAS). At slow to medium MAS frequencies, significant residual line broadening is observed. The technical advances in the field of MAS during the past decade has resulted in very fast spinning frequencies (up to 150 kHz), however, the obtained resolution is still not sufficient for all applications (Agarwal et al., 2014; Andreas et al., 2016; Penzel et al., 2019; Stöppler et al., 2018). The residual linewidth in a fully protonated protein sample is still 100-200 Hz, making *de-novo* resonance assignment and structure determination from proton-detected spectra challenging.

Field Code Changed

Field Code Changed

To further reduce the residual linewidth especially at slow to medium range MAS frequencies (lower than 60 kHz), homonuclear decoupling sequences can be employed. The first strategy to average out homonuclear proton-proton interactions using radio-frequency (rf) fields in static samples was suggested by Lee and Goldburg (Goldburg and Lee, 1963; Lee and Goldburg, 1965). Since then, many homonuclear decoupling sequences have been developed including solid-echo based sequences (WAHUHA (Waugh et al., 1968), MREV (Mansfield and Grannell, 1971; Rhim et al., 1973), BR-24 (Burum and Rhim, 1979a, 1979b)), time-reversal sequences (Rhim et al., 1971), C- and R-symmetry based sequences (Levitt, 2007; Madhu et al., 2001; Paul et al., 2010), tilted magic-echo-based sequences (Gan et al., 2011; Lu et al., 2012; Nishiyama et al., 2012), and computer-optimized sequences like DUMBO (Grimminck et al., 2011; Halse and Emsley, 2012; Sakellariou et al., 2000; Salager et al., 2009). Each of these sequences has their own advantages and disadvantages in terms of robustness for different MAS spinning regimes and requirements for the radio-frequency field strength. Several examples of these types of sequences and their performance can be found in a recent review (Mote et al., 2016) and will not be discussed in detail.

The theoretical basis of the Lee-Goldburg sequence relies on the manipulation of the spin interactions by an off-resonance irradiation such that the quantization axis of the effective field is along the magic angle in a rotating frame (Lee and Goldburg, 1965). This leads to the removal of all second-rank interactions in spin space, i.e., the dipolar coupling, to second order in static samples. The Lee-Goldburg pulse sequence has undergone a lot of modification to be more robust and to compensate pulse errors generated by the spectrometer hardware. It was later also combined with magic-angle spinning where interference between averaging in real and in spin space becomes an issue (Mote et al., 2016; Vinogradov et al., 2004). Well-known alterations of the pulse sequence include the frequency-switched Lee-Goldburg (FSLG) (Bielecki et al., 1990; Levitt et al., 1993; Mehring and Waugh, 1972a) or the phase-modulated Lee-Goldburg (PMLG) sequences (Vinogradov et al., 1999, 2000, 2001, 2004). Various super cycles have been developed to compensate higher-order terms and pulse errors. The most commonly used super cycles or alterations include an inversion of the phase ramp ($PMLG_{x\bar{x}}$) (Leskes et al., 2007; Paul et al., 2009) or a relative phase shift between two PMLG cycles with an inversion of the second cycle (LG-4) (Halse et al., 2014; Halse and Emsley, 2013). These super cycles have the disadvantage of reducing the scaling factors of the chemical shifts leading to reduced separation of the lines assuming similar decoupling efficiency. The advantage of such super-cycled sequences is the suppression of artefacts (quadrature images, axial peaks, and spurious signals) in the spectrum (Bosman et al., 2004).

The theoretical description of Lee-Goldburg sequences can be done within the framework of average Hamiltonian theory (AHT) (Ernst et al., 1990; Haeberlen, 1976) or Floquet theory (Leskes et al., 2009, 2010; Scholz et al., 2010; Shirley, 1965). Such a description has been used to predict the first-order resonance conditions between the MAS frequency and the modulation frequency of the pulse sequence as well as the magnitude of the non-vanishing second-order dipole-dipole cross terms. The second-order cross terms are one source of the residual linewidth that is still observed after homonuclear decoupling and they need to be minimized in order to obtain narrow spectral lines (Vinogradov et al., 2004). A further factor for the performance degradation in FSLG sequences was believed to be experimental imperfections caused either by rf-field inhomogeneity or pulse transients (Barbara et al., 1991; Mehring and Waugh, 1972b), which, in certain cases, were also used

Field Code Changed
Field Code Changed
Field Code Changed
Field Code Changed
Field Code Changed
Formatted: English (US)
Field Code Changed
Field Code Changed
Field Code Changed
Field Code Changed
Field Code Changed
Field Code Changed
Field Code Changed
Field Code Changed
Field Code Changed
Field Code Changed
Field Code Changed
Field Code Changed
Field Code Changed

for the improvement of the performance of the pulse sequence (Vega, 2004). It was shown that changing the phase transients by changing the tuning of the probe can be used to improve the spectral quality obtained by an S2-DUMBO sequences (Brouwer and Horvath, 2015).

In this article, we investigate the influence of multiple parameters on the residual linewidth in FSLG decoupled spectra. We characterize the magnitude of the broadening by pulse transients for a standard FSLG sequence and compare the results to an implementation using transient-compensated pulses (Hellwagner et al., 2018; Tabuchi et al., 2010; Takeda et al., 2009; Wittmann et al., 2015, 2016). Furthermore, we analyze the FSLG sequence theoretically using Floquet theory up to third-order. We are able to show that third-order terms play an important role in strongly-coupled systems like CH_2 groups. We present FSLG-based experiments using transient-compensated pulses on model compounds where homonuclear dipolar second-order terms are purposefully minimized to illustrate the importance of the third-order contribution. Additionally, we investigate the broadening due to rf-field inhomogeneity by comparing results from restricted samples and numerical simulations taking the rf-field distribution over the sample into account. We show that the rf-field inhomogeneity is the main source of line broadening in FSLG-based experiments due to the dependence of the chemical-shift scaling on the rf-field amplitude. The distribution of rf fields leads to a difference in scaled isotropic chemical shifts depending on the characteristics of the generated B_1 field and causes the dominant contribution to the residual broadening FSLG decoupled spectra.

2 Theory

The Lee-Goldburg scheme is based on averaging the second-rank spin tensor of a homonuclear dipolar Hamiltonian by rotating it around a field oriented along the magic angle. Such an averaging scheme is related to the removal of the spatial second-rank tensors of the Hamiltonian by MAS. The magic-angle irradiation is achieved by applying an off-resonance rf-Hamiltonian of the general form

$$\mathcal{H} = \Delta\omega I_z + \omega_1 I_x \qquad (1)$$

where the off-resonance term $\Delta\omega$ is defined as $\omega_0 - \omega_{rf}$ with ω_0 denoting the Larmor frequency of protons. The combination of the offset and a constant rf irradiation along the x-axis generates a quantization axis which is tilted by the angle θ defined by

$$\theta = \tan^{-1}\left(\frac{\omega_1}{\Delta\omega}\right). \qquad (2)$$

It can be shown that in first-order average Hamiltonian theory the homonuclear dipole-dipole interactions vanish if θ is adjusted to the magic angle. As a consequence, the chemical-shift Hamiltonian is also scaled down by a factor $d^{(1)}_{0,0}(-\theta) = \cos\theta$ which takes a value of around 0.577 at $\theta = 54.7°$. An equivalent description of off-resonance irradiation can be achieved by a phase modulation of the radio-frequency irradiation of the form:

Field Code Changed
Field Code Changed
Field Code Changed
Field Code Changed
Field Code Changed
Field Code Changed
Field Code Changed
Field Code Changed
Field Code Changed
Field Code Changed
Formatted: Font: Do not check spelling or grammar
Deleted: 2

$$\mathcal{H}_{\mathrm{rf}}(t) = \omega_1 \sum_p (\cos(\varphi(t)) I_{px}). \quad (3)$$

Here, ω_1 represents a constant rf-amplitude and $\varphi(t)$ a linear phase ramp.

The arguments based on AHT only hold true in a static regime but to get a full understanding of the sequence under MAS, the interference with the sample rotation has to be considered. The analysis of Hamiltonians with multiple time dependencies that are not commensurate is done best using Floquet theory (Leskes et al., 2010; Scholz et al., 2010).

The Floquet analysis is done in an interaction frame of the rf-field Hamiltonian where the interaction-frame transformation is defined by the propagator

$$\hat{U}_{\mathrm{rf}}(t) = \hat{T} \exp\left(-i \int_0^t \mathcal{H}_{\mathrm{rf}}(t')dt'\right) \quad (4)$$

with the interaction-frame Hamiltonian given by

$$\tilde{\mathcal{H}}(t) = \hat{U}_{\mathrm{rf}}^{-1}(t) \mathcal{H}(t) \hat{U}_{\mathrm{rf}}(t). \quad (5)$$

Here, $\hat{T}$ represents the Dyson time-ordering operator (Dyson, 1949). The spherical spin-tensor operators of rank r under a generalized interaction-frame transformation will transform according to

$$\tilde{T}_{r,0}(t) = \sum_{s=-r}^{r} a_{r,s}(t) T_{r,s} = \sum_{s=-r}^{r} T_{r,s} \sum_{k=-\infty}^{\infty} \sum_{\ell=-s}^{s} a_{r,s}^{(k,\ell)} e^{i(k\omega_{\mathrm{m}} + \ell\omega_{\mathrm{eff}})t} \quad (6)$$

where ω_{m} is the modulation frequency of the sequence and ω_{eff} is the effective nutation frequency of a basic pulse element. Here, the scaling factors $a_{r,s}^{(k,\ell)}$ are the Fourier coefficients of the interaction-frame trajectory. These two frequencies together with the MAS frequency ω_{r} constitute the three basic frequencies that characterize the time dependence of the Hamiltonian. Note, that for an ideal FSLG sequence the effective nutation frequency will be zero. Hence, the interaction-frame Hamiltonian can be written as a Fourier series

$$\tilde{\mathcal{H}}(t) = \sum_{n=-2}^{2} \sum_{k=-\infty}^{\infty} \sum_{\ell=-2}^{2} \tilde{\mathcal{H}}^{(n,k,\ell)} e^{in\omega_{\mathrm{r}}t} e^{ik\omega_{\mathrm{m}}t} e^{i\ell\omega_{\mathrm{eff}}t}. \quad (7)$$

A set of possible resonance conditions can be derived for any set of integers (n_0, k_0, ℓ_0) that fulfill the equation

$$n_0\omega_{\mathrm{r}} + k_0\omega_{\mathrm{m}} + \ell_0\omega_{\mathrm{eff}} = 0. \quad (8)$$

Since decoupling sequences are mostly applied outside of any resonance conditions and the residual linewidth is dominated by residual couplings, we will only focus on non-resonant terms where the effective Hamiltonian is given by

Formatted: Font: Do not check spelling or grammar
Field Code Changed
Deleted: 3
Field Code Changed
Field Code Changed
Formatted: Font: Do not check spelling or grammar
Deleted: 4
Field Code Changed
Formatted: Font: Do not check spelling or grammar
Deleted: 5
Field Code Changed
Field Code Changed
Field Code Changed
Formatted: Font: Do not check spelling or grammar
Deleted: 6
Field Code Changed
Field Code Changed
Field Code Changed
Field Code Changed
Field Code Changed
Field Code Changed
Formatted: Font: Do not check spelling or grammar
Deleted: 7
Field Code Changed
Formatted: Font: Do not check spelling or grammar
Deleted: 8

$$\bar{\mathcal{H}} = \tilde{\mathcal{H}}_{(1)}^{(0,0,0)} + \tilde{\mathcal{H}}_{(2)}^{(0,0,0)} + \tilde{\mathcal{H}}_{(3)}^{(0,0,0)} + \cdots \quad (9)$$

with

$$\tilde{\mathcal{H}}_{(1)}^{(0,0,0)} = \tilde{\mathcal{H}}^{(0,0,0)} \quad (10)$$

the second-order effective Hamiltonian defined by

$$\tilde{\mathcal{H}}_{(2)}^{(0,0,0)} = \sum_{\nu,\kappa,\lambda} -\frac{1}{2}\frac{\left[\tilde{\mathcal{H}}^{(-\nu,-\kappa,-\lambda)}, \tilde{\mathcal{H}}^{(\nu,\kappa,\lambda)}\right]}{\nu\omega_{\mathrm{r}} + \kappa\omega_{\mathrm{m}} + \lambda\omega_{\mathrm{eff}}} \quad (11)$$

and the third-order component given by

$$\tilde{\mathcal{H}}_{(3)}^{(0,0,0)} = \sum_{\nu,\kappa,\lambda}\sum_{n_0',k_0',l_0'} \frac{1}{2}\frac{\left[\left[\tilde{\mathcal{H}}^{(\nu,\kappa,\lambda)}, \tilde{\mathcal{H}}^{(n_0',k_0',l_0')}\right], \tilde{\mathcal{H}}^{(-\nu-n_0',-\kappa-k_0',-\lambda-l_0')}\right]}{(\nu\omega_{\mathrm{r}} + \kappa\omega_{\mathrm{m}} + \lambda\omega_{\mathrm{eff}})^2}$$

$$+ \sum_{\nu,\kappa,\lambda}\sum_{\nu',\kappa',\lambda'} \frac{1}{3}\frac{\left[\tilde{\mathcal{H}}^{(\nu,\kappa,\lambda)}, \left[\tilde{\mathcal{H}}^{(\nu',\kappa',\lambda')}, \tilde{\mathcal{H}}^{(-\nu-\nu',-\kappa-\kappa',-\lambda-\lambda')},\right]\right]}{(\nu\omega_{\mathrm{r}} + \kappa\omega_{\mathrm{m}} + \lambda\omega_{\mathrm{eff}})(\nu'\omega_{\mathrm{r}} + \kappa'\omega_{\mathrm{m}} + \lambda'\omega_{\mathrm{eff}})}. \quad (12)$$

The summations in the third-order term have to be restricted to values of $(\nu, \nu', \kappa, \kappa', \lambda, \lambda')$ that fulfill the inequalities $\nu\omega_{\mathrm{r}} + \kappa\omega_{\mathrm{m}} + \lambda\omega_{\mathrm{eff}} \neq 0$ and $\nu'\omega_{\mathrm{r}} + \kappa'\omega_{\mathrm{m}} + \lambda'\omega_{\mathrm{eff}} \neq 0$. Note that the equation for the third-order contribution differs from the original paper due to a sign mistake in the original work (Ernst et al., 2005). To the best of our knowledge, only one theoretical description of third-order terms under simultaneous rf-irradiation and MAS (Tatton et al., 2012) has been published. These terms were shown to cause a shift of the resonance frequency. Evaluation of these expressions for homonuclear dipolar coupled Hamiltonians under FSLG irradiation provides insight into terms that are not averaged out and can contribute to the residual linewidth of the spectrum. A detailed analysis of the individual contributions and their behavior under the pulse sequence is presented in the following section.

3 Analytical and Numerical Results

The analytical calculation of the second-order cross terms for a homonuclear coupled three-spin systems with two non-vanishing dipolar couplings $\delta_{1,2}$ and $\delta_{1,3}$ yields lengthy expressions that depend on the powder angles α and β as well as the relative orientation of the two couplings Φ and the angle of the effective field θ with respect to the external magnetic field which is set to the magic angle for a standard FSLG sequence. All of these terms scale linearly with the product of the two dipolar-coupling constants $\delta_{1,2}\delta_{1,3}$. In order to illustrate the symmetry of the remaining terms, the Hamiltonian is projected on all possible three-spin tensor operators. The three-spin operators are defined according to reference (Garon et al., 2015) where they were first derived. The projections are calculated for powder angles $\alpha = \beta = 45°$ and a relative dipole orientation $\Phi =$

Formatted: Font: Do not check spelling or grammar
Deleted: 9
Field Code Changed
Field Code Changed
Formatted: Font: Do not check spelling or grammar
Deleted: 10
Formatted: Font: Do not check spelling or grammar
Deleted: 11
Field Code Changed
Field Code Changed
Formatted: Font: Do not check spelling or grammar
Deleted: 12
Field Code Changed
Deleted: qualitative
Field Code Changed
Field Code Changed

45° since many of the terms have a local maximum at this set of angles. The modulation frequency of the pulse sequence was set to be ten times larger than the MAS frequency to avoid any possible resonance conditions in the calculations. The ratio of the modulation and the MAS frequency will be noted as $z = \omega_m/\omega_r$. The second-order cross terms between two dipolar couplings with one spin in common lead to spin-tensor operators of rank zero to three. Figure 1 shows the dependence of these

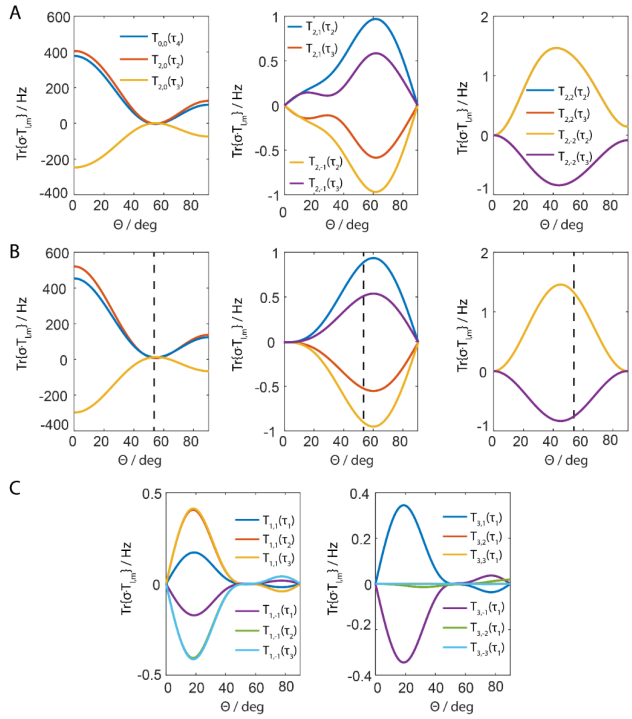

Figure 1: Projection of the magnitude of the three-spin tensor operators of the second-order effective Hamiltonian from analytical calculations (B) or numerical simulations (A and C). A and B show the same tensor components, which are comparable in magnitude. The effective Hamiltonian was calculated for a Lee-Goldburg type irradiation scheme with a $(2\pi)(-2\pi)$ rotation about the effective field angle θ. For the calculations a Hamiltonian with two homonuclear dipolar couplings was assumed and the powder values were set to $\alpha = \beta = 45°$ and the relative orientation of the dipoles to $\Phi = 45°$ with the dipolar couplings set to $\delta_{1,2}$=10 kHz and $\delta_{1,3}$=20 kHz. The ratio of the modulation frequency of the pulse sequence and the MAS frequency was assumed to be 10 in order to avoid higher-order contributions to the numerical simulations. It is obvious from the magnitude of the tensor components that only the $T_{0,0}(\tau_4)$ and the $T_{2,0}(\tau_2)$ and $T_{2,0}(\tau_3)$ terms are relevant but they exhibit a broad minimum centered around the magic angle, which is indicated by the black dashed line. For a definition of the three-spin spherical-tensor operators, see Ref. (Garon et al., 2015).

Formatted: Font: Not Bold
Deleted: Figure 1
Field Code Changed
Field Code Changed
Deleted: r
Deleted:
Deleted: (Garon et al., 2015)

second-order three-spin cross terms as a function of the effective-field angle of the FSLG irradiation. The dominant terms are the $T_{0,0}(\tau_4) = \frac{2}{\sqrt{3}}\left(I_{1x}I_{2y}I_{3z} - I_{1x}I_{2z}I_{3y} - I_{1y}I_{2x}I_{3z} + I_{1y}I_{2z}I_{3x} + I_{1z}I_{2x}I_{3y} - I_{1z}I_{2y}I_{3x}\right)$ and the $T_{2,0}(\tau_2) = \sqrt{2}\left(I_{1y}I_{2z}I_{3x} + I_{1z}I_{2y}I_{3x} - I_{1x}I_{2z}I_{3y} - I_{1z}I_{2x}I_{3y}\right)$ and $T_{2,0}(\tau_3) = \sqrt{\frac{2}{3}}\left(-2I_{1x}I_{2y}I_{3z} - I_{1x}I_{2z}I_{3y} + I_{1z}I_{2x}I_{3y} + 2I_{1y}I_{2x}I_{3z} + I_{1y}I_{2z}I_{3x} - I_{1z}I_{2y}I_{3x}\right)$ tensor operators where we follow the definition and notation introduced in Ref. (Garon et al., 2015). They all arise from commutators of one homonuclear dipolar coupling in the interaction frame of the effective field with another dipolar coupling where one spin is in common. The dependence on the effective-field angle θ can be expressed by a combination of Legendre polynomials of zeroth, second, and fourth order indicating that the origin of the terms is indeed second order and a product of two spatial second-rank tensors. In order to verify the analytical calculations, full numerical simulations (using the spin simulation environment GAMMA (Smith et al., 1994)) using the same set of parameters were run to calculate the effective Hamiltonian numerically over a full rotor period. The numerical effective Hamiltonian was also projected onto the relevant spin-tensor operators which led to very similar but not identical values for the coefficients of the tensor operators (compare Figure 1A and Figure 1B showing the same tensor components). The differences are explained as follows: In Figure 1A and C, all non-zero terms from numerical simulations are shown but analytical calculations only result in $T_{0,0}$ and $T_{2,0}$ terms (Figure 1B). The tensor components $T_{1,m}$ and $T_{3,m}$ only appear in the numerical simulations (Figure 1C) and originate from higher-order contributions that are not considered in the analytical calculations. The significant contributions ($T_{1,0}$ terms) to the second-order three-spin terms are minimized around the orientation of the effective field along the magic angle while the remaining terms ($T_{l,m}$ terms with $m \neq 0$) are all very small. The minimum appears to be very broad and, therefore, it is expected that the sequence is fairly robust towards maladjustments in the rf-field amplitude or the phase ramp which would result in a change of the effective field angle.

In order to investigate other possible contributions to the residual linewidth that are not averaged out by the combination of MAS and the FSLG-based pulse sequence, third-order terms of a single dipolar coupling in a two-spin system were analyzed (for numerical expression of the third-order effective Hamiltonian, see the Supplementary Information). These terms are expected to scale with $\delta_{1,2}^3$ since they result from double-commutator terms due to their third-order origin. Under MAS without simultaneous rf irradiation, such terms are averaged out since a single dipolar coupling commutes with itself at all times. This is no longer true under rf irradiation. Evaluating the double commutators for all non-resonant terms and analyzing the resulting effective Hamiltonian, only terms with the tensor symmetry $T_{2,m}$ remain. The analytical expressions for these terms can be found in the Supporting Information. The magnitude and dependence on the effective-field angle are shown in Figure 2. It can be concluded from these calculations that the terms are not averaged out by a FSLG irradiation with the angle of the effective field set to the magic angle but rather around 60° for the $T_{2,0}$ term and around 40° for the $T_{2,\pm2}$ term. The $T_{2,\pm1}$ term does not show a local minimum around typical effective-field angles but calculations of the propagation of the density operator under such a term show that it does not result in an effective line broadening but rather in a shift of the resonance frequency. This

Deleted: ¶

Deleted:

Deleted: (Garon et al., 2015)

Field Code Changed
Field Code Changed
Formatted: Font: Not Bold
Deleted: Figure 1
Field Code Changed
Formatted: Font: Not Bold
Deleted: Figure 1
Field Code Changed
Formatted: Font: Not Bold
Deleted: Figure 1
Field Code Changed
Field Code Changed
Field Code Changed
Formatted: Font: Not Bold
Deleted: Figure 1
Field Code Changed
Field Code Changed
Field Code Changed
Formatted: Font: Not Bold
Deleted: Figure 1
Field Code Changed
Field Code Changed
Field Code Changed
Field Code Changed
Formatted: Font: Not Bold
Deleted: Figure 2
Field Code Changed
Field Code Changed
Field Code Changed

fact does not hold true for the $T_{2,0}$ and the $T_{2,\pm2}$ terms which ultimately contribute to the linewidth under FSLG. The magnitude and angle dependence of these spin-tensors elements is shown in Figure 2B and they were again calculated for the angle values

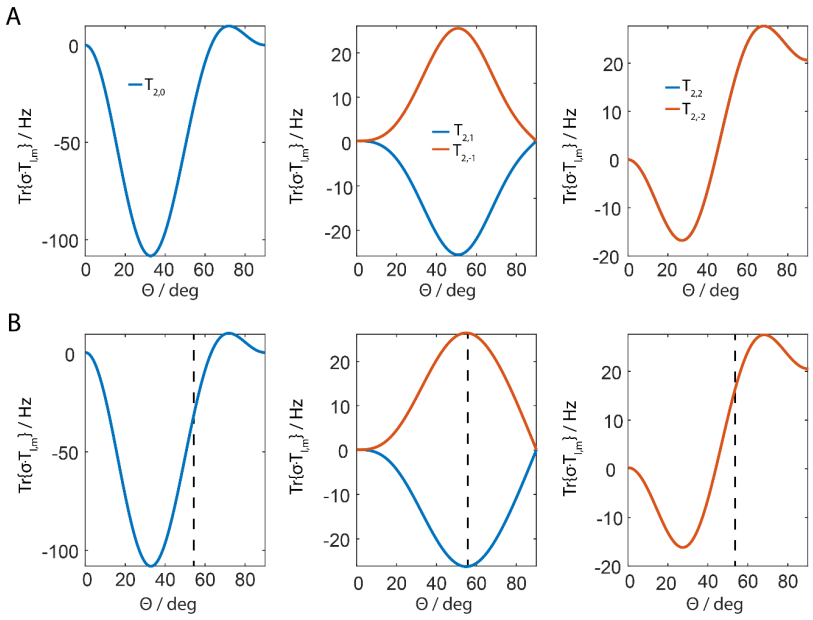

Figure 2: Magnitude of the third-order spin-tensor operators resulting after FSLG-irradiation only assuming a single homonuclear dipolar coupling from numerical simulations (A) and analytical calculations (B) showing the same tensor components. The simulation parameters for the powder orientations and the MAS to modulation frequency ratio are the same as shown in Figure 1. The remaining terms vanish either around 60° for the $\boldsymbol{T_{2,0}}$ and around 40° for the $\boldsymbol{T_{2,\pm2}}$ term. It is interesting to note that with the traditional FSLG scheme none of the third-order terms vanishes.

$\alpha = \beta = 45°$, $\Phi = 45°$, and a value of $z = 10$. The dipolar coupling was set to 40 kHz which is representative for a CH_2-group that remains one of the biggest challenges in homonuclear decoupling. The effective-field strength was set to 125 kHz and it can be shown that the magnitude of the third-order terms scales down quadratically with the effective field assuming the same ratio $z = \omega_m/\omega_r$. However, rf-field amplitudes higher than 100 kHz are often experimentally not feasible for many practical applications.

Field Code Changed
Field Code Changed
Formatted: Font: Not Bold
Deleted: Figure 2
Field Code Changed
Field Code Changed
Formatted: Font:
Deleted: Figure 1
Field Code Changed
Field Code Changed

It is obvious from Figure 2, that the third-order terms (double commutator terms of a single homonuclear dipolar coupling in the interaction frame of the effective field) do not vanish under FSLG-irradiation and they are significant in size given that the $T_{2,0} = \frac{1}{\sqrt{6}}\left(3I_{1z}I_{2z} - \left(\vec{I}_1 \cdot \vec{I}_2\right)\right)$ and the $T_{2,\pm 2} = \frac{1}{2}\left(I_1^{\pm} \cdot I_2^{\pm}\right)$ contribute directly to the residual line broadening. We believe that these third-order terms contribute significantly to the residual linewidth under FSLG decoupling especially for strongly coupled spins as encountered in CH_2-groups. As in the case of the second-order cross terms, there is a good agreement between the analytical (Fig. 2B) and the numerical calculations (Fig. 2A) of the third-order terms.

The influence of heteronuclear dipolar couplings on the residual line broadening can be analyzed theoretically in the same way. Again, third-order terms from a single heteronuclear dipolar coupling are obtained and do not vanish if the effective-field angle is set to the magic angle. These terms have the same spin-tensor components as the third-order homonuclear terms but the spatial dependence differs. The dependence on the effective field angle is shown in the Supporting Information (Figure S2). The second-order heteronuclear-homonuclear dipolar cross terms show a similar behavior as the homonuclear-homonuclear terms. Their functional form is shown in Figure S3 of the SI. They are minimized for an effective field orientation around the magic angle.

Further line broadening during the FSLG sequence can come from experimental errors like sample inhomogeneities, pulse transients, and B_1-field inhomogeneities.

4 Transient Compensation in FSLG

In order to compensate pulse transients during the FSLG pulse sequence, small modifications have to be made to the implementation of the sequence. On the spectrometer, the sequence is typically implemented as a rectangular pulse of constant amplitude but with discrete phase steps. The new spectrometer hardware can generate shape files with a time resolution of 50 ns and an almost perfect phase ramp can be realized in order to generate a constant offset irradiation. Nevertheless, due to the finite bandwidth of the resonance circuit, a finite rise time of the pulse is observed as well as phase transients at the start of the pulse and at the positions of the 180° phase jump. To compensate for these pulse transients, a finite edge of the pulse has to be introduced. As a consequence of this pulse edge, the flip angle of the shaped pulse is no longer 2π and the amplitude has to be corrected. Using a linear phase ramp will lead to an effective-field angle that is not constant throughout the sequence. Therefore, the phase ramp has to be calculated explicitly by numerical integration of the required offset of the irradiation that is needed in combination with the time-dependent rf-field amplitude to generate a constant effective-field direction and a 2π rotation about the effective field.

The phase of the shaped pulse is defined as

$$\Phi(t) = \int_0^t \Delta\nu(t)\, dt \qquad (13)$$

with the offset frequency $\Delta\nu$ defined by

Formatted: Font: Not Bold
Field Code Changed
Deleted: Figure 2
Field Code Changed
Field Code Changed
Deleted: 13
Field Code Changed
Formatted: Font: Do not check spelling or grammar

$$\Delta\nu(t) = \sqrt{\nu_{\text{eff}}^2 - \nu_1^2} = \nu_1(t)\cot\theta. \quad (14)$$

The rf-field amplitude ν_1 is defined by the shape and the length of the pulse. The implementation of the pulse sequence for shaped and rectangular pulses is shown in Figure 3. The shape of the phase ramp can be explained by considering the functional

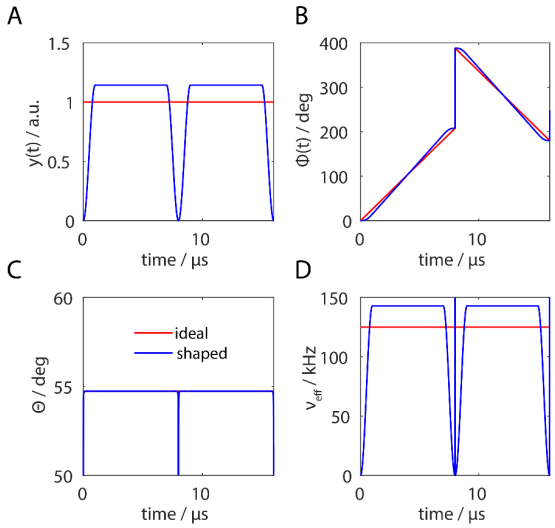

Figure 3: Representation of possible implementation for FSLG decoupling with shaped pulses guaranteeing a constant effective-field angle. In red, the ideal FSLG pulse sequence is shown assuming rectangular pulses and blue, the implementation of shaped pulses. A) Flip-angle corrected amplitude with finite pulse edges of 0.4 µs. B) Time-dependent phase ramp with a 180° phase jump for the second pulse. C) Resulting effective-field angle which is kept constant at the magic angle for both implementations. D) Resulting effective field which corresponds to a net rotation of 2π at 125 kHz.

form of the pulse edge which corresponds to a sine function. Therefore, the phase ramp during the pulse edges must correspond to a cosine function and the slope in the constant part is steeper compared to rectangular pulses to compensate for reduced effective rotation during the finite edge.

In order to validate the theoretical consideration of the pulse sequence, numerical simulations in a homonuclear three-spin systems were performed with both pulse implementations shown in Figure 3. To validate the contributions of second- and third-order terms discussed in the theory section, simulations using only one ($\delta_{12} \neq 0$) and two non-zero dipolar couplings ($\delta_{12} \neq 0,\ \delta_{13} \neq 0$) in a three-spin system were performed. The average effective field was set to be 125 kHz corresponding to a Lee-Goldburg pulse length for a full 2π nutation of 8 µs. The MAS frequency was set to be 6.25 kHz leading to a ratio of

Deleted: 14
Formatted: Font: Do not check spelling or grammar
Field Code Changed
Field Code Changed
Field Code Changed
Deleted: Figure 3
Field Code Changed
Formatted: Font: 10 pt
Field Code Changed
Field Code Changed
Formatted: Font: 10 pt
Deleted: Figure 3
Deleted: , respectively,

$z = 10$. Powder averaging was used according to the ZCW scheme with 300 crystal orientations (Cheng et al., 1973). A relative orientation of $\Phi = 45°$ was used for the two dipole tensors. The residual splitting as a function of the effective field direction is shown in Figure 4 without taking chemical-shift correction into account. Therefore, the

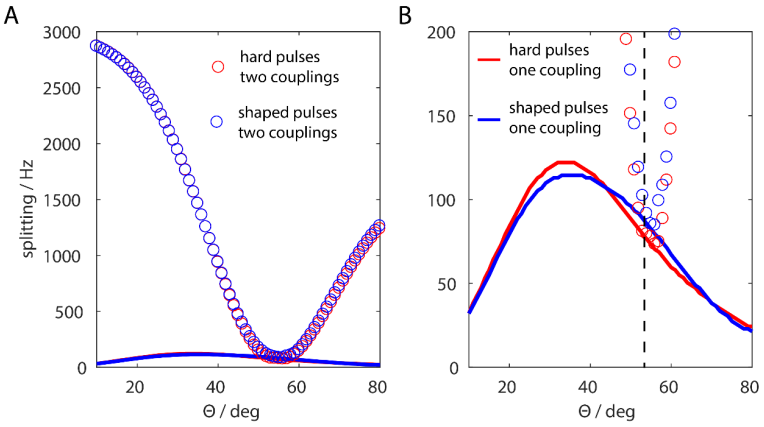

Figure 4: Calculated residual splitting of FSLG sequence in a homonuclear three-spin system as a dependence of the effective-field angle and implementations using rectangular pulses (red) and shaped pulses (blue). The splitting due to the residual coupling is shown without chemical-shift scaling due to the effective field axis. The second-order cross terms are minimized around the magic angle (circles) but the third-order terms resulting from a single dipolar coupling are never fully removed (solid line). A) Full scale of splitting as a function of the effective-field angle. B) Zoom on the residual splitting contributions up to 200 Hz. The MAS frequency was set to 6.25 kHz, the effective field to 125 kHz, the relative dipole orientation to 45°, the dipolar couplings to 40 kHz for the single coupling and to 10 kHz for the second coupling, and powder averaging was applied. The black dashed line represents $\theta = \theta_{ma}$.

splitting represents the residual effective coupling in the Hamiltonian. It is obvious that the shaped-pulse implementation and the rectangular pulses lead to very similar linewidths and dependences on the effective-field angle θ. Furthermore, these results demonstrate the fact that the second-order three-spin terms are averaged out fairly well around the magic angle but that there are still significant contributions from third-order terms. These third-order terms are a combination of the functional forms shown in Figure 2 for the $T_{2,0}$ and the $T_{2,\pm2}$ tensor operators.

Considering the chemical-shift scaling for residual linewidths, the third-order terms are minimized around an effective-field angle of around 60°. This effective-field angle dependence was also demonstrated experimentally and the results are shown in Figure 5.

Field Code Changed
Field Code Changed
Formatted: Font: 10 pt
Deleted: Figure 4
Field Code Changed
Field Code Changed
Deleted: Simulations
Deleted: of
Deleted: linewidth
Deleted: presented
Deleted: correction
Deleted: linewidths
Deleted: line-width
Field Code Changed
Formatted: Font: Not Bold
Deleted: Figure 2
Field Code Changed
Field Code Changed
Field Code Changed
Field Code Changed
Formatted: Font: 10 pt
Deleted: Figure 5

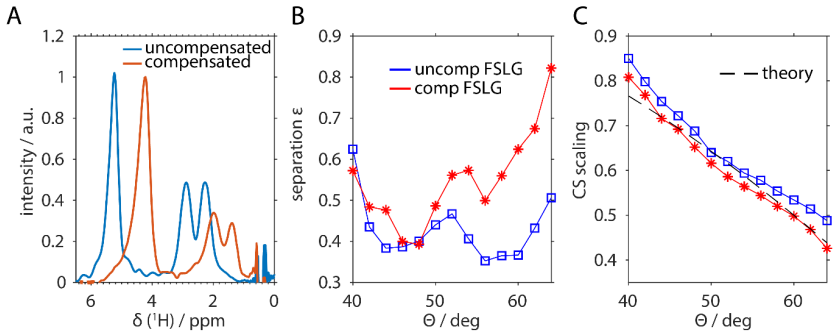

Figure 5: Experimental results of FSLG based decoupling on U-^{13}C-^{15}N-glycine as a function of the effective-field angle. The spectra using rectangular pulses and compensated pulses during the FSLG block are shown in A with the effective-field angle set to the magic angle $\theta = \theta_{m}$. The spectra are not processed in terms of chemical-shift scaling and referencing to illustrate the effect of implementing compensated pulses. The decoupling performance is analyzed in terms of the splitting between the two resonance lines of the CH_2-group (B) defined by the separation parameter ε and the chemical-shift scaling factor (C). The MAS frequency was set to 14 kHz with an effective field of 125 kHz at an external magnetic field of 14.1 T.

Field Code Changed

Field Code Changed

5 Experimental Results

Experiments were performed on various glycine derivatives designed to illustrate the different contributions to the residual linewidth under FSLG decoupling. In order to avoid unexpected effects due to windowed PMLG detection during the decoupling period (Vinogradov et al., 2002), the experiments were implemented as 2D experiments with the FSLG decoupling in the indirect dimension followed by either a long CP for carbon detection or direct proton detection. The CP time was chosen to be 3 ms to ensure transfer from all protons in natural abundance glycine and to minimize the effects of heteronuclear dipolar couplings in natural abundance samples. Since proton spin diffusion is very efficient at the low MAS frequency that was used in our measurements, we expect that also magnetization from protons bound to ^{12}C is observed. Additionally, simple FSLG sequences without a super cycle were used to benefit from the maximum chemical-shift scaling. Therefore, quadrature images and axial peaks were observed in the indirect dimension, which were discarded for the analysis. Figure 5 shows a comparison of the decoupling efficiency using transient-compensated pulses and conventional rectangular pulses. The dependence of the linewidth on the effective-field angle was investigated in the range from 40° to 65°. The experiments were performed on a uniformly labelled ^{13}C-^{15}N-glycine at an external magnetic field of 14.1 T using an effective field of 125 kHz and MAS spinning speed of 14 kHz. The quantity that was used to judge the decoupling efficiency was the separation of the two proton signals of the CH_2-group. The separation parameter is defined by the ratio of the intensity between the two lines and the

Field Code Changed

Field Code Changed

Formatted: Font: 10 pt

Deleted: Figure 5

intensity of the two lines $\varepsilon = \frac{2I_{\min,H}}{(I_{\max,H1}+I_{\max,H2})}$ (see Supporting Information Figure S6 for a graphical representation of the parameters). A value of 0 corresponds to baseline separation of the two lines whereas a value of 1 represents indistinguishable lines. Figure 5B shows this splitting as a function of the effective-field angle and it can be seen that the transient-compensated FSLG sequences perform slightly worse than the conventional rectangular pulses but the differences are small. Furthermore, it is shown in the figure that the optimum decoupling efficiency is not exactly at the magic angle but shifted to slightly higher angles. This agrees with the theoretical predictions that the third-order terms, which are believed to be significant in a CH_2-group, are minimized around higher values of ca. 60°. A further observation of these experiments is the behavior of the chemical-shift scaling. The use of compensated pulses leads to chemical-shift scaling factors that agree very well with the theoretical prediction of $\cos\theta$, whereas rectangular pulses lead to higher chemical-shift scaling (Figure 5C).

A further contribution to the residual linewidth is the heteronuclear dipolar coupling, which can be avoided to a large degree by using natural abundance samples. The influence of the heteronuclear coupling was investigated by recording the spectra of natural abundance glycine using compensated and rectangular pulses. The resulting spectra for an effective-field angle of $\theta = \theta_m$ and 60° are shown in Figure 6A and B, respectively. The improvement is significant compared to the labelled compound

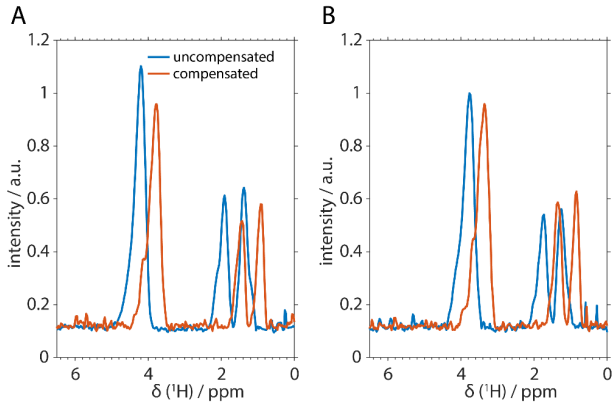

Figure 6: Experimental spectra of FSLG based decoupling on natural abundance glycine. The spectra are not processed in terms of chemical-shift scaling and referencing to illustrate the effect of implementing compensated pulses. The effective-field angle was either set to the magic angle (A) or 60° (B). The shift in resonance frequencies between the uncompensated pulses (blue) and the compensated (red) can be attributed to additional effective fields caused by pulse transients. The MAS frequency was set to 14 kHz with an effective field of 125 kHz at an external magnetic field of 14.1 T.

since in all implementations the separation of the CH_2-group is almost at the baseline (compare to Figure 5A). Quantifying the linewidth (without chemical-shift scaling), an improvement of ~60 Hz is observed going from fully-labelled to unlabeled

Field Code Changed
Field Code Changed
Deleted: Figure 5
Formatted: Font: 10 pt
Deleted: Figure 5
Field Code Changed
Field Code Changed
Formatted: Font: 10 pt
Field Code Changed
Field Code Changed
Formatted: Font: 10 pt
Deleted: Figure 6
Field Code Changed
Deleted: Figure 5
Field Code Changed
Formatted: Font: 10 pt

samples. This agrees well with the theoretical calculations of heteronuclear third-order terms shown in Figure S2 and previous results (Tatton et al., 2012).

It can be argued from the spectra shown in Figure 6 that the compensation leads to slightly narrower CH_2-resonances. However, this improvement is still within the range of experimental uncertainties. Note, that the spectra are shown without post-processing, i.e. chemical-shift scaling and relative referencing. It is interesting to observe that the whole spectrum shifts to lower ppm-values for the compensated implementation (Figures 5A and 6). Based on numerical simulations, we believe this to be due to the better compensation of the effective nutation over a full FSLG cycle and the additional removal of fictitious fields (second-order one-spin terms) by applying transient compensation (Ernst et al., 2005; Hellwagner et al., 2017). The effect of changing the effective-field angle from the magic angle to 60° is very small and is hard to judge from the spectra.

Experimental quantification of the relative size of the second- and third-order terms was implemented by designing and synthesizing glycine derivatives that contain an isolated two-spin system as well as a multi-spin system. A deuterated d_8-2-^{13}C-^{15}N-glycine ethylester (see Fig. 7A) with a protonated CH_2-group was synthesized to represent an isolated ^1H-^1H spin

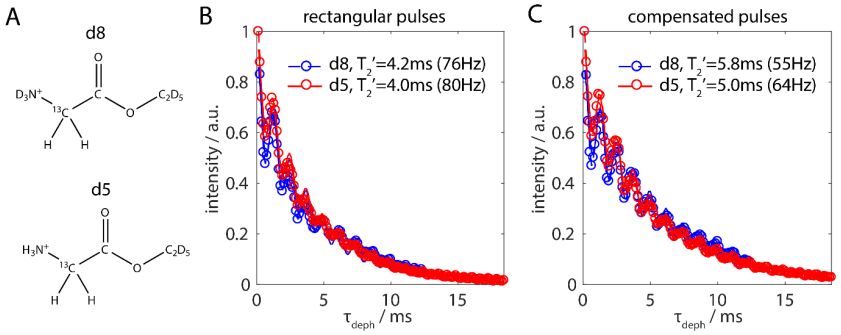

Figure 7: Quantification of the second- and third-order error terms in the FSLG pulse sequence. A) Model compounds of glycine ethylester with an isolated CH_2-spin system (d8) and protonated representing a multi-spin system (d5). B) T_2' decay curves of the CH_2-signal using FSLG decoupling on the protons during the echo time with rectangular pulses during the echo period and an effective-field angle equal to the magic angle. C) The identical curves to B) but using compensated pulses. The corresponding full width at half maximum is given in the figure legend. The MAS frequency was set to 14 kHz with an effective field of 125 kHz at an external magnetic field of 14.1 T.

system. In full analogy, a deuterated d_5-2-^{13}C-^{15}N-glycine ethylester with a protonated CH_2- and a NH_3^+-group (see Fig. 7A) was used as a multi-spin model system. Hahn-Echo sequences with FSLG-based decoupling during the echo time were recorded and the T_2'-times were extracted. The oscillations in the decay curves have been observed before and could, according to the literature, be removed by a double-echo sequence (Paruzzo et al., 2018).

It can be seen from Figure 7 that the influence of the second-order terms is very small and only contributes about 5-10% of the effective proton T_2' times. The dominating terms are identified to be the third-order auto term since they make up most of the

Formatted: Font: 10 pt
Deleted: Figure 6
Field Code Changed
Field Code Changed
Field Code Changed
Field Code Changed
Field Code Changed
Formatted: Font: 10 pt
Deleted: Figure 7
Field Code Changed

non refocusable residual linewidth when comparing a two-spin to a multi-spin system. Furthermore, the quantification of the decoupling performance leads to the conclusion that the pulse-transient compensation does improve the decoupling efficiency by 20-30% in terms of refocusable linewidth. Nevertheless, as shown before, this effect is hardly visible in the directly detected spectra but pulse-transient compensation leads to higher predictability of the sequence.

The huge discrepancy in directly detected linewidth (~400 Hz for the N-H peak of natural abundance glycine, see Fig. 6) and the refocusable terms (55-80 Hz, see Fig. 7B and C) needs to be explained by other effects. In order to study the effect of the time-independent part of the rf-field inhomogeneity under MAS, samples in 2.5 mm o.d. Bruker rotors were packed by filling different parts of the rotor. We have not included phase- or amplitude-modulations generated by MAS due to rf-field inhomogeneity in our investigation (Goldman and Tekely, 2001; Levitt et al., 1988; Tekely and Goldman, 2001; Tosner et al., 2018). Five rotors each of adamantane and natural abundance glycine were packed using either a full rotor, the upper third (*up*), the bottom third (*low*), the middle third (*mid*), and a very small part in the middle of the rotor (*center*). The remaining rotor volume was filled with Teflon spacers. The distribution of the ^{1}H rf field over the active sample volume was determined by measuring nutation curves using the adamantane sample with direct detection of the proton signal. Subsequent Fourier transformation of the nutation curves yields a distribution profile of the rf fields within the probe. These profiles are shown in the Supporting Information (Figure S7). The maxima of the rf-profile are consistently at higher values than the calibrated rf-field amplitudes of 100 kHz. The calibration was done on a full rotor by determining the first zero crossing of a π pulse. These shifted maxima are due to the very broad distribution of rf-field amplitudes in the full rotor and the large drawn out foot towards low rf fields. The profiles of the restricted samples show that this foot is mostly observed in the outer thirds of the rotor, whereas the middle as well as the center part is narrowed down around the maximum. The sum of the middle, upper, and lower part of the rotor compares very well to the profile of the full rotor. However, the integral of the distribution is slightly higher by a factor of 1.1, which is either due to spacers that do not cover exactly a third of the rotor, or looser packing in the full sample.

These profiles have been used in further studies to investigate the influence of the rf-field distribution on the decoupling efficiency. Numerical simulations were performed using an eight-spin system with characteristic couplings and shifts similar to the ones found in glycine (spin system details can be found in the SI, Tables S1 and S2) under FSLG decoupling using a distribution of rf-field amplitudes as observed in the nutation experiments. These simulations are compared with FSLG experiments that were performed on the restricted natural abundance glycine samples. The comparison of the numerical simulations and experimental results are shown in Figure 8.

Deleted: static

Deleted: f

Field Code Changed

Deleted: teflon

Field Code Changed

Formatted: Font: Not Bold

Deleted: Figure 8

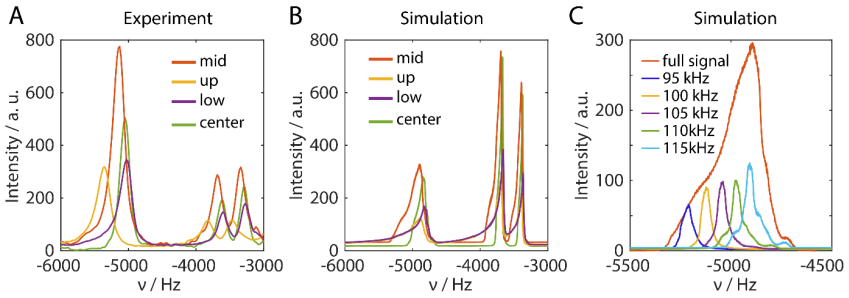

Figure 8: A) Experimental spectra of natural abundance glycine using FSLG decoupling in the indirect dimension. The packing schemes correspond to the adamantane samples. B) Simulated proton spectra of natural abundance glycine using an 8-spin system as input. The different contributions of the rotor to the total spectra are shown in different colours that match Figure S7. The rf-field resolution was 500 Hz using the rf profiles measured on adamantane. The frequency axis is not an absolute axis and only the spacing between the peaks is correct. The linewidth and relative intensities of the NH_3^+-peaks are comparable. The single outlier is the relative intensity of the middle third compared to the center packed rotor. However, this might be due to slightly different packing in the adamantane and the glycine. C) Simulated NH_3^+-peak of the sample restricted to the middle third showing the contribution to the total linewidth of the weighted lines of different rf-field amplitudes. An rf-field range of 2 kHz was used for each of the rf-field amplitudes generating a linewidth of around 30 Hz. The total linewidth is dominated by the isotropic chemical-shift distribution due to the variation in the scaling factors.

Field Code Changed

Table 1: Tabulated values of the linewidths at half maximum of the simulated and experimental spectra of natural abundance glycine. The values are extracted from the spectra shown in Figure 8 and are without chemical-shift correction. In order to obtain the real value, they have to be divided by a factor of 0.57.

Field Code Changed

Deleted: Figure 8

Field Code Changed

	Middle	Centre	Upper	Lower
Δ_{sim} / Hz	196	168	365	226
Δ_{exp} / Hz	220	174	225	252

The measured linewidths for the simulations and experiments are listed in Table 1. The full width at half maximum (FWHM) obtained from the simulations compare well with the experiments. The relative intensities of the NH_3^+-peaks for different packing is also reproduced fairly well with small discrepancies for the center-packed and the middle-third rotor. One problem in the experimental spectra is the phase correction as well as the baseline correction. Due to the very broad and drawn out rf profile, the simulated peak has a large foot to higher chemical shifts. Such an asymmetric peak can be corrected by a zeroth-order phase correction to obtain a more symmetric looking line shape. This phase correction can lead to a distortion of the relative intensity as well as the extracted linewidth.

Field Code Changed

Formatted: Font: Not Bold

Deleted: Table 1

Further data that can be extracted from the simulations is the inherent linewidth that remains due to insufficient decoupling strength at various rf fields. This can be interpreted and compared with an experimentally determined T_2'. The inherent

linewidth from the numerical simulations was obtained by correcting the respective rf-field values for the chemical-shift scaling. The superimposed linewidth was fitted and was found to be about 35 Hz for the NH_3^+-peak of glycine corresponding to T_2'=10 ms. This compares well to observed values in the literature (Paruzzo et al., 2018).

6 Material and Methods

Numerical simulations were performed using the GAMMA spin-simulation environment (Smith et al., 1994). Different crystallites were simulated with 300 ZCW orientations for powder averaging (Cheng et al., 1973). The single-crystal orientations are specified in the text. The MAS frequency was set to 6.25 kHz for all the simulations and analytical calculations with an effective-field strength of 125 kHz.

The analytical calculations were done in Mathematica by transforming the dipolar Hamiltonian into a tilted-frame with the effective-field angle. Then, the rf-field interaction-frame transformation of the Hamiltonian was calculated by $(2\pi)(-2\pi)$ rotation around the tilted axis. The effective Hamiltonians were calculated according to Eqs. (11) and (12). The decomposition of the Hamiltonian was done by projecting the Hamiltonian on the two- or three-spin spherical tensor operators.

The glycine ethylester derivatives were synthesized starting from 2-^{13}C-^{15}N-glycine (purchased from Sigma Aldrich) with d_6-ethanol (anhydr.) by dropwise addition of $SOCl_2$ at 0°C. After 2h under reflux conditions, the reaction mixture was rinsed with toluene and subsequent removal of the solvent under vacuum led to d_8-2-^{13}C-^{15}N-glycineethylester as a highly crystalline white powder. In order to synthesize the d_5-2-^{13}C-^{15}N-glycineethylester, the d_8-glycineethylester was treated with methanol in an ultrasonic bath to exchange the amine protons. Removal of residual solvent under vacuum yielded a white crystalline powder.

The experiments were all carried out on a 14.1 T magnet (600 MHz proton resonance frequency) on a Bruker Avance III HD spectrometer using a 2.5 mm triple-resonance Bruker probe. The probe was modified with a pick-up coil to perform transient compensation and the trap was removed to operate the probe in double-resonance mode. All rotors were completely filled without sample restriction except where stated explicitly. Processing was done in Topspin (Bruker Biospin, Rheinstetten, Germany) and zeroth- and first-order phase corrections were applied manually after Fourier transformation. All spectra were recorded as 2D spectra with protons in the indirect dimension to employ windowless decoupling. The transient compensation was performed as described in Ref. (Wittmann et al., 2016). The quality of the transient compensation was monitored by measuring the phase and the amplitude of the radio-frequency field using the pick-up coil. Transient-compensated pulses showed only minor deviations in phase and amplitude from the intended pulse shape.

7 Conclusion

In conclusion, we investigated the different contributions to the residual line broadening in FSLG decoupled proton spectra and tried to quantify their magnitude. The most important factor was found to be the rf-field inhomogeneity that contributes to about 75% of the linewidth even if the sample is restricted in the center of the rotor. This is a result of a distribution of

Field Code Changed
Field Code Changed
Field Code Changed
Deleted: (12)
Formatted: Font: Do not check spelling or grammar
Formatted: Font: Do not check spelling or grammar
Field Code Changed
Deleted: (11)
Field Code Changed
Deleted: E
Formatted: Not Superscript/ Subscript
Deleted: M
Field Code Changed

chemical-shift scaling factors due to different effective-field directions in different parts of the sample. The outer parts of the rotor do not contribute much to the observed spectrum and typically represent themselves as a foot in the peak due to the low rf fields at the edges of the coil. A further confirmation that the rf-field inhomogeneity is the main source of the residual linewidth is the fact that the use of higher effective fields does not result in better signal resolution. Second- and third-order error terms scale down linearly or quadratically with the effective-field strength but this was not observed experimentally. The relative rf-field distribution in the coil is always the same independently of the magnitude of the rf-field. Therefore, the chemical-shift scaling and the resulting spectra are expected to show little change with an increase in the rf-field amplitude. Since the rf-field inhomogeneity is the main contribution to the residual linewidth, improved performance is only expected if the probe design is improved so that the rf-field profile is more homogeneous over the whole sample.

We have also shown that pulse transients do not contribute significantly to the residual linewidth, but generate a shift of the spectrum, which makes it more difficult to interpret the results and achieve a reliable frequency calibration. Removal of phase transients and adaption of the pulse sequence led to more predictable results in terms of chemical-shift scaling and smaller variations of the shift on the frequency axis. Furthermore, it was shown theoretically and by numerical simulations that homonuclear third-order terms contribute strongly to the residual homogeneous linewidth. These terms cannot be removed by altering the sequence, e.g. changing the angle of the effective field, as they do not exhibit the same spatial behavior as second-order three-spin terms. Small improvements were found by changing the effective-field angle to slightly higher values of around 60°, which can be understood theoretically, but the spectral quality still remains too broad to be useful for many practical applications.

Deleted: absolute values

Acknowledgment

We would like to thank F.M. Paruzzo, Prof. Dr. P.K. Madhu and Dr. K. Mote for insightful discussions about theory and experimental implementation of homonuclear decoupling. This work was supported by the Swiss National Science Foundation (grants 200020_169879, 200020_159707 and 200020_188988) and the ETH Zurich (grant ETH-10 15-1). B.M acknowledges support by the European Research Council (ERC) under the European Union's Horizon 2020 research and innovation program (grant agreement n° 741863, FASTER).

References

Agarwal, V., Penzel, S., Szekely, K., Cadalbert, R., Testori, E., Oss, A., Past, J., Samoson, A., Ernst, M., Böckmann, A. and Meier, B. H.: DeNovo 3D Structure Determination from Sub-milligram Protein Samples by Solid-State 100kHz MAS NMR Spectroscopy, Angew. Chemie - Int. Ed., 53(45), 12253–12256, doi:10.1002/anie.201405730, 2014.

Andreas, L. B., Jaudzems, K., Stanek, J., Lalli, D., Bertarello, A., Le Marchand, T., Cala-De Paepe, D., Kotelovica, S., Akopjana, I., Knott, B., Wegner, S., Engelke, F., Lesage, A., Emsley, L., Tars, K., Herrmann, T. and Pintacuda, G.: Structure

of fully protonated proteins by proton-detected magic-angle spinning NMR, Proc. Natl. Acad. Sci., 113(33), 9187–9192, doi:10.1073/pnas.1602248113, 2016.

Barbara, T. M., Martin, J. F. and Wurl, J. G.: Phase transients in NMR probe circuits, J. Magn. Reson., 93(3), 497–508, doi:10.1016/0022-2364(91)90078-8, 1991.

Barfield, M.: Structural dependencies of interresidue scalar coupling h3JNC′ and donor 1H chemical shifts in the hydrogen bonding regions of proteins, J. Am. Chem. Soc., 124(15), 4158–4168, doi:10.1021/ja012674v, 2002.

Berglund, B. and Vaughan, R. W.: Correlations between proton chemical shift tensors, deuterium quadrupole couplings, and bond distances for hydrogen bonds in solids, J. Chem. Phys., 73(5), 2037–2043, doi:10.1063/1.440423, 1980.

Bielecki, A., Kolbert, A. C., De Groot, H. J. M., Griffin, R. G. and Levitt, M. H.: Frequency-Switched Lee—Goldburg Sequences in Solids, ACADEMIC PRESS, INC., 1990.

Bosman, L., Madhu, P. K., Vega, S. and Vinogradov, E.: Improvement of homonuclear dipolar decoupling sequences in solid-state nuclear magnetic resonance utilising radiofrequency imperfections, J. Magn. Reson., 169(1), 39–48, doi:10.1016/j.jmr.2004.04.001, 2004.

Brouwer, D. H. and Horvath, M.: Minimizing the effects of RF inhomogeneity and phase transients allows resolution of two peaks in the 1H CRAMPS NMR spectrum of adamantane, Solid State Nucl. Magn. Reson., 71, 30–40, doi:10.1016/j.ssnmr.2015.10.005, 2015.

Burum, D. P. and Rhim, W. K.: An improved NMR technique for homonuclear dipolar decoupling in solids: Application to polycrystalline ice, J. Chem. Phys., 70(7), 3553–3554, doi:10.1063/1.437892, 1979a.

Burum, D. P. and Rhim, W. K.: Analysis of multiple pulse NMR in solids. III, J. Chem. Phys., 71(2), 944–956, doi:10.1063/1.438385, 1979b.

Cheng, V. B., Suzukawa, H. H. and Wolfsberg, M.: Investigations of a nonrandom numerical method for multidimensional integration, J. Chem. Phys., 59(8), 3992–3999, doi:10.1063/1.1680590, 1973.

Dyson, F. J.: The radiation theories of Tomonaga, Schwinger, and Feynman, Phys. Rev., 75(3), 486–502, doi:10.1103/PhysRev.75.486, 1949.

Ernst, M., Samoson, A. and Meier, B. H.: Decoupling and recoupling using continuous-wave irradiation in magic-angle-spinning solid-state NMR: A unified description using bimodal Floquet theory, J. Chem. Phys., 123(6), doi:10.1063/1.1944291, 2005.

Ernst, R. R., Bodenhausen, G. and Wokaun, A.: Principles of Nuclear Magnetic Resonance in One and Two Dimensions, Oxford University., 1990.

Gan, Z., Madhu, P. K., Amoureux, J. P., Trébosc, J. and Lafon, O.: A tunable homonuclear dipolar decoupling scheme for high-resolution proton NMR of solids from slow to fast magic-angle spinning, Chem. Phys. Lett., 503(1–3), 167–170, doi:10.1016/j.cplett.2010.12.070, 2011.

Garon, A., Zeier, R. and Glaser, S. J.: Visualizing operators of coupled spin systems, Phys. Rev. A - At. Mol. Opt. Phys., 91(4), 1–28, doi:10.1103/PhysRevA.91.042122, 2015.

Goldburg, W. I. and Lee, M.: Nuclear magnetic resonance line narrowing by a rotating rf field, Phys. Rev. Lett., 11(6), 255–258, doi:10.1103/PhysRevLett.11.255, 1963.

Goldman, M. and Tekely, P.: Effect of radial RF field on MAS spectra, Comptes Rendus l'Academie des Sci. - Ser. IIc Chem., 4(11), 795–800, doi:10.1016/S1387-1609(01)01310-X, 2001.

Grimminck, D. L. A. G., Vasa, S. K., Meerts, W. L., Kentgens, A. P. M. and Brinkmann, A.: EASY-GOING DUMBO on-spectrometer optimisation of phase modulated homonuclear decoupling sequences in solid-state NMR, Chem. Phys. Lett., 509(4–6), 186–191, doi:10.1016/j.cplett.2011.04.079, 2011.

Haeberlen, U.: High Resolution NMR in Solids: Selective Averaging, Academic Press., 1976.

Halse, M. E. and Emsley, L.: A common theory for phase-modulated homonuclear decoupling in solid-state NMR, Phys. Chem. Chem. Phys., 14, 9121–9130, doi:10.1039/c2cp40720e, 2012.

Halse, M. E. and Emsley, L.: Improved phase-modulated homonuclear dipolar decoupling for solid-state NMR spectroscopy from symmetry considerations, J. Phys. Chem. A, 117(25), 5280–5290, doi:10.1021/jp4038733, 2013.

Halse, M. E., Schlagnitweit, J. and Emsley, L.: High-resolution1H solid-state NMR spectroscopy using windowed LG4 homonuclear dipolar decoupling, Isr. J. Chem., 54(1–2), 136–146, doi:10.1002/ijch.201300101, 2014.

Hellwagner, J., Sharma, K., Tan, K. O., Wittmann, J. J., Meier, B. H., Madhu, P. K. and Ernst, M.: Optimizing symmetry-based recoupling sequences in solid-state NMR by pulse-transient compensation and asynchronous implementation, J. Chem. Phys., 146(24), doi:10.1063/1.4989542, 2017.

Hellwagner, J., Wili, N., Ibáñez, L. F., Wittmann, J. J., Meier, B. H. and Ernst, M.: Transient effects in π-pulse sequences in MAS solid-state NMR, J. Magn. Reson., 287, 65–73, doi:10.1016/j.jmr.2017.12.015, 2018.

Lee, M. and Goldburg, W. I.: Nuclear-magnetic-resonance line narrowing by a rotating rf field, Phys. Rev., 140(4A), 1261–1271, doi:10.1103/PhysRev.140.A1261, 1965.

Leskes, M., Madhu, P. K. and Vega, S.: A broad-banded z-rotation windowed phase-modulated Lee-Goldburg pulse sequence for 1H spectroscopy in solid-state NMR, Chem. Phys. Lett., 447(4–6), 370–374, doi:10.1016/j.cplett.2007.09.041, 2007.

Leskes, M., Madhu, P. K. and Vega, S.: Why does PMLG proton decoupling work at 65 kHz MAS?, J. Magn. Reson., 199(2), 208–213, doi:10.1016/j.jmr.2009.05.003, 2009.

Leskes, M., Madhu, P. K. and Vega, S.: Floquet theory in solid-state nuclear magnetic resonance, Prog. Nucl. Magn. Reson. Spectrosc., 57(4), 345–380, doi:10.1016/j.pnmrs.2010.06.002, 2010.

Levitt, M. H.: Symmetry-Based Pulse Sequences in Magic-Angle Spinning Solid-State NMR, in Encyclopedia of Magnetic Resonance, vol. 9, pp. 165–196., 2007.

Levitt, M. H., Oas, T. G. and Griffin, R. G.: Rotary Resonance Recoupling in Heteronuclear Spin Pair Systems, Isr. J. Chem., 28(4), 271–282, doi:10.1002/ijch.198800039, 1988.

Levitt, M. H., Kolbert, A. C., Bielecki, A. and Ruben, D. J.: High-resolution 1H NMR in solids with frequency-switched multiple-pulse sequences, Solid State Nucl. Magn. Reson., 2(4), 151–163, doi:https://doi.org/10.1016/0926-2040(93)90021-E, 1993.

Lu, X., Lafon, O., Trébosc, J., Thankamony, A. S. L., Nishiyama, Y., Gan, Z., Madhu, P. K. and Amoureux, J. P.: Detailed analysis of the TIMES and TIMES 0 high-resolution MAS methods for high-resolution proton NMR, J. Magn. Reson., 223, 219–227, doi:10.1016/j.jmr.2012.07.015, 2012.

Madhu, P. K., Zhao, X. and Levitt, M. H.: High-resolution1H NMR in the solid state using symmetry-based pulse sequences, Chem. Phys. Lett., 346(1–2), 142–148, doi:10.1016/S0009-2614(01)00876-4, 2001.

Mansfield, P. and Grannell, A. B.: Improved resolution of small resonance shifts of dilute nuclear spin systems in solids by pulsed double resonance, J. Phys. C Solid State Phys., 4(10), doi:10.1088/0022-3719/4/10/005, 1971.

Mehring, M. and Waugh, J. S.: Magic-angle NMR experiments in solids, Phys. Rev. B, 5(9), 3459–3471, doi:10.1103/PhysRevB.5.3459, 1972a.

Mehring, M. and Waugh, J. S.: Phase transients in pulsed NMR spectrometers, Rev. Sci. Instrum., 43(4), 649–653, doi:10.1063/1.1685714, 1972b.

Mote, K. R., Agarwal, V. and Madhu, P. K.: Five decades of homonuclear dipolar decoupling in solid-state NMR: Status and outlook, Prog. Nucl. Magn. Reson. Spectrosc., 97, 1–39, doi:10.1016/j.pnmrs.2016.08.001, 2016.

Nishiyama, Y., Lu, X., Trébosc, J., Lafon, O., Gan, Z., Madhu, P. K. and Amoureux, J. P.: Practical choice of 1 H- 1 H decoupling schemes in through-bond 1 H-{X} HMQC experiments at ultra-fast MAS, J. Magn. Reson., 214, 151–158, doi:10.1016/j.jmr.2011.10.014, 2012.

Parker, L. L., Houk, A. R. and Jensen, J. H.: Cooperative hydrogen bonding effects are key determinants of backbone amide proton chemical shifts in proteins, J. Am. Chem. Soc., 128(30), 9863–9872, doi:10.1021/ja0617901, 2006.

Paruzzo, F. M., Stevanato, G., Halse, M. E., Schlagnitweit, J., Mammoli, D., Lesage, A. and Emsley, L.: Refocused linewidths less than 10 Hz in1H solid-state NMR, J. Magn. Reson., 293, 41–46, doi:10.1016/j.jmr.2018.06.001, 2018.

Paul, S., Thakur, R. S., Goswami, M., Sauerwein, A. C., Mamone, S., Concistrè, M., Förster, H., Levitt, M. H. and Madhu, P. K.: Supercycled homonuclear dipolar decoupling sequences in solid-state NMR, J. Magn. Reson., 197(1), 14–19, doi:10.1016/j.jmr.2008.11.011, 2009.

Paul, S., Schneider, D. and Madhu, P. K.: 1H Homonuclear dipolar decoupling using symmetry-based pulse sequences at ultra fast magic-angle spinning frequencies, J. Magn. Reson., 206(2), 241–245, doi:10.1016/j.jmr.2010.07.013, 2010.

Penzel, S., Oss, A., Org, M. L., Samoson, A., Böckmann, A., Ernst, M. and Meier, B. H.: Spinning faster: protein NMR at MAS frequencies up to 126 kHz, J. Biomol. NMR, 73(1–2), 19–29, doi:10.1007/s10858-018-0219-9, 2019.

Rhim, W.-K., Elleman, D. D. and Vaughan, R. W.: Analysis of multiple pulse NMR in solids, J. Chem. Phys., 59(11), 3740–3749, doi:10.1063/1.1680545, 1973.

Rhim, W. -K., Pines, A. and Waugh, J. S.: Time-Reversal Experiments in Dipolar-Coupled Spin Systems, Phys. Rev. B, 3, 684–696, 1971.

Sakellariou, D., Lesage, A., Hodgkinson, P. and Emsley, L.: Homonuclear dipolar decoupling in solid-state NMR using continuous phase modulation, Chem. Phys. Lett., 319(3–4), 253–260, doi:10.1016/S0009-2614(00)00127-5, 2000.

Salager, E., Stein, R. S., Steuernagel, S., Lesage, A., Elena, B. and Emsley, L.: Enhanced sensitivity in high-resolution 1H

615 solid-state NMR spectroscopy with DUMBO dipolar decoupling under ultra-fast MAS, Chem. Phys. Lett., 469(4–6), 336–341, doi:10.1016/j.cplett.2008.12.073, 2009.

Scholz, I., Van Beek, J. D. and Ernst, M.: Operator-based Floquet theory in solid-state NMR, Solid State Nucl. Magn. Reson., 37(3–4), 39–59, doi:10.1016/j.ssnmr.2010.04.003, 2010.

Shirley, J. H.: Solution of the schrödinger equation with a hamiltonian periodic in time, Phys. Rev., 138(4B), 620 doi:10.1103/PhysRev.138.B979, 1965.

Smith, S. A., Levante, T. O., Meier, B. H. and Ernst, R. R.: Computer Simulations in Magnetic Resonance. An Object-Oriented Programming Approach, J. Magn. Reson. Ser. A, 106(1), 75–105, doi:10.1006/jmra.1994.1008, 1994.

Stöppler, D., Macpherson, A., Smith-Penzel, S., Basse, N., Lecomte, F., Deboves, H., Taylor, R. D., Norman, T., Porter, J., Waters, L. C., Westwood, M., Cossins, B., Cain, K., White, J., Griffin, R., Prosser, C., Kelm, S., Sullivan, A. H., Fox, D., Carr, 625 M. D., Henry, A., Taylor, R., Meier, B. H., Oschkinat, H. and Lawson, A. D.: Insight into small molecule binding to the neonatal Fc receptor by X-ray crystallography and 100 kHz magic-angle-spinning NMR, PLoS Biol., 16(5), 1–27, doi:10.1371/journal.pbio.2006192, 2018.

Tabuchi, Y., Negoro, M., Takeda, K. and Kitagawa, M.: Total compensation of pulse transients inside a resonator, J. Magn. Reson., 204(2), 327–332, doi:10.1016/j.jmr.2010.03.014, 2010.

630 Takeda, K., Tabuchi, Y., Negoro, M. and Kitagawa, M.: Active compensation of rf-pulse transients, J. Magn. Reson., 197(2), 242–244, doi:10.1016/j.jmr.2008.12.012, 2009.

Tatton, A. S., Frantsuzov, I., Brown, S. P. and Hodgkinson, P.: Unexpected effects of third-order cross-terms in heteronuclear spin systems under simultaneous radio-frequency irradiation and magic-angle spinning NMR, J. Chem. Phys., 136(8), doi:10.1063/1.3684879, 2012.

635 Tekely, P. and Goldman, M.: Radial-field sidebands in MAS, J. Magn. Reson., 148(1), 135–141, doi:10.1006/jmre.2000.2215, 2001.

Tosner, Z., Sarkar, R., Becker-Baldus, J., Glaubitz, C., Wegner, S., Engelke, F., Glaser, S. J. and Reif, B.: Overcoming volume selectivity of dipolar recoupling in biological solid-state NMR, Angew. Chemie Int. Ed., 2, 14514–14518, doi:10.1016/0165-1838(81)90062-X, 2018.

640 Vega, A. J.: Controlling the effects of pulse transients and RF inhomogeneity in phase-modulated multiple-pulse sequences for homonuclear decoupling in solid-state proton NMR, J. Magn. Reson., 170(1), 22–41, doi:10.1016/j.jmr.2004.05.017, 2004.

Vinogradov, E., Madhu, P. K. K. and Vega, S.: High-resolution proton solid-state NMR spectroscopy by phase-modulated Lee–Goldburg experiment, Chem. Phys. Lett., 314(5–6), 443–450, doi:10.1016/S0009-2614(99)01174-4, 1999.

Vinogradov, E., Madhu, P. K. and Vega, S.: A bimodal Floquet analysis of phase modulated Lee-Goldburg high resolution 645 proton magic angle spinning NMR experiments, Chem. Phys. Lett., 329(3–4), 207–214, doi:10.1016/S0009-2614(00)01006-X, 2000.

Vinogradov, E., Madhu, P. K. and Vega, S.: Phase modulated Lee-Goldburg magic angle spinning proton nuclear magnetic resonance experiments in the solid state: A bimodal Floquet theoretical treatment, J. Chem. Phys., 115(19), 8983–9000,

doi:10.1063/1.1408287, 2001.

Vinogradov, E., Madhu, P. K. and Vega, S.: Proton spectroscopy in solid state nuclear magnetic resonance with windowed phase modulated Lee-Goldburg decoupling sequences, Chem. Phys. Lett., 354(3–4), 193–202, doi:10.1016/S0009-2614(02)00060-X, 2002.

Vinogradov, E., Madhu, P. K. and Vega, S.: Strategies for high-resolution proton spectroscopy in solid-state NMR., Top. Curr. Chem., 246, 33–90, doi:10.1007/b98648, 2004.

Waugh, J. S., Huber, L. M. and Haeberlen, U.: Approach to high-resolution NMR in solids, Phys. Rev. Lett., 20(5), 180–182, doi:10.1103/PhysRevLett.20.180, 1968.

Wittmann, J. J., Takeda, K., Meier, B. H. and Ernst, M.: Compensating pulse imperfections in solid-state NMR spectroscopy: A key to better reproducibility and performance, Angew. Chemie - Int. Ed., 54(43), 12592–12596, doi:10.1002/anie.201504782, 2015.

Wittmann, J. J., Mertens, V., Takeda, K., Meier, B. H. and Ernst, M.: Quantification and compensation of the influence of pulse transients on symmetry-based recoupling sequences, J. Magn. Reson., 263, 7–18, doi:10.1016/j.jmr.2015.12.011, 2016.